

Near-infrared frequency-domain optical spectroscopy and magnetic resonance imaging: a combined approach to studying cerebral maturation in neonatal rabbits

H. E. D'Arceuil

Neuroradiology Section
Martinos Center for Biomedical Imaging
Room 2301, Building 149, 13th Street
Charlestown, Massachusetts 02129
E-mail: helen@nmr.mgh.harvard.edu

M. P. Hotakainen

Martinos Center for Biomedical Imaging
Department of Radiology
Massachusetts General Hospital
Charlestown, Massachusetts
and
Cognitive Brain Research Unit
Department of Psychology
University of Helsinki, Finland

C. Liu

G. Themelis

Martinos Center for Biomedical Imaging
Department of Radiology
Massachusetts General Hospital
Charlestown, Massachusetts

A. J. de Crespigny

Neuroradiology Section
Martinos Center for Biomedical Imaging
Department of Radiology
Massachusetts General Hospital
Charlestown, Massachusetts

M. A. Franceschini

Martinos Center for Biomedical Imaging
Department of Radiology
Massachusetts General Hospital
Charlestown, Massachusetts

1 Introduction

The brain of the newborn human is immature at birth and it continues to mature postnatally both structurally and physiologically. In premature infants (24 to 32 weeks gestation), the brain undergoes the following changes: cortical layering (all six layers of the cortex are formed), myelination and myelin maturation, neural organization (neuronal alignment, orientation, layering), proliferation of dendrites, and formation of synapses.¹ The cortical vascularity is developed before the subcortical vascularity and the cortical vessels have abundant anastomotic channels supplying the cortex.

Currently there is no technology that enables easy, continuous, safe, and noninvasive monitoring of human brain devel-

Abstract. The neonatal rabbit brain shows prolonged postnatal development both structurally and physiologically. We use noninvasive near-IR frequency-domain optical spectroscopy (NIRS) and magnetic resonance imaging (MRI) to follow early developmental changes in cerebral oxygenation and anatomy, respectively. Four groups of animals are measured: NIRS in normals, MRI in normals, and both NIRS and MRI with hypoxia-ischemia (HI) (diffusion MRI staging). NIRS and/or MRI are performed from *P*3 (postnatal day=*P*) up to *P*76. NIRS is performed on awake animals with a frequency-domain tissue photometer. Absolute values of oxyhemoglobin concentration ($[HbO_2]$), deoxyhemoglobin concentration ($[HbR]$), total hemoglobin concentration (HbT), and hemoglobin saturation (StO_2) are calculated. The brains of all animals appeared to be maturing as shown in the diffusion tensor MRI. Mean optical coefficients (reduced scattering) remained unchanged in all animals throughout. StO_2 increased in all animals (40% at *P*9 to 65% at *P*43) and there are no differences between normal, HI controls, and HI brains. The measured increase in StO_2 is in agreement with the reported increase in blood flow during the first 2 months of life in rabbits. HbT, which reflects blood volume, peaked at postnatal day *P*17, as expected since the capillary density increases up to *P*17 when the microvasculature matures. © 2005 Society of Photo-Optical Instrumentation Engineers. [DOI: 10.1117/1.1852554]

Keywords: magnetic resonance imaging; diffusion; brain maturation; hemoglobin concentration; hemoglobin saturation; frequency-domain; optical spectroscopy; near infrared.

Paper NEU-08 received Feb. 25, 2004; revised manuscript received Jun. 14, 2004; accepted for publication Jun. 18, 2004; published online Jan. 31, 2005.

opment and that provides functional and metabolic information. Near-IR spectroscopy (NIRS) can acquire measures of cerebral oxygenation in real time, which is especially suitable for measurements in all neonates. Positron emission tomography (PET) studies in humans have shown regional changes of glucose utilization, oxygen consumption, and blood flow with brain maturation.²⁻⁷ However, because these studies require intravenous injection of radioactive tracers, this methodology, even though noninvasive, can be justified for use in human neonates only in a diagnostic capacity where the benefit to be gained from its diagnostic ability outweighs the inherent risk to the patient from using this technology. PET studies are not ethically justified in normal human neonates. NIRS and magnetic resonance imaging (MRI) both hold appeal for brain development studies because they are safe and noninvasive. In the past 2 decades, NIRS has been tested as a means to

Address all correspondence to H. E. D'Arceuil, Neuroradiology Section, Martinos Center for Biomedical Imaging, Room 2301, Building 149, 13th Street, Charlestown, MA 02129; Tel: 617-726-8005; Fax: 617-726-7422; E-mail: helen@nmr.mgh.harvard.edu

monitor the brain's cerebral oxygenation status^{8–11} and to investigate brain function^{12–15} in neonates. MRI has been used to assess brain maturation in preterm infants.^{16–23} Also, a handful of functional MRI (fMRI) studies of neonates have shown an age-dependent change in the functional signal response to visual stimulation.^{24–29}

Longitudinal MRI studies of human neonates are rare.³⁰ While human newborns within the first 2 postnatal weeks can be fed, swaddled, and put to sleep then into the MR scanner, older neonates are usually scanned at night or during their nap time. The scans on the older neonates are therefore more labor intensive and less successful and more often involve sedation of the infants to prevent motion artifacts in the images. Because of the need for anesthesia, frequent MRI measurements on human neonates and infants are less desirable unless there is a diagnostic or prognostic need.

To investigate the sensitivity of NIRS to hemoglobin changes due to brain development, a large number of measurements on several subjects over a long period of time is required. To our knowledge, there are no optical studies that have tested the reproducibility of optical measurements in such an extensive way as has been done in this study. Brain maturation in the neonatal rabbit was an ideal *in vivo* system to interrogate to verify that our optical measurements were reproducible and to investigate hemoglobin changes during brain development from birth to adolescence.

As stated, the neonatal rabbit's brain is immature at birth and is comparable to a preterm human fetus of approximately 26 to 34-weeks gestation. The neonatal rabbit's brain also shows prolonged postnatal development and mimics some aspects of the human preterm brain in the way it reacts to various brain insults such as hypoxia and hypoxia ischemia.^{31–33} Structurally, myelination continues in the corpus callosum, internal capsule, and the centrum semiovale up to the fourth postpartum week. In addition, physiological changes such as increases in local cerebral blood flow,³¹ capillary density,^{34,35} oxidative metabolism, and glucose utilization³⁶ occur in tandem with these structural changes.

In our study, we used both NIRS and MRI to investigate cerebral vascular maturation and microstructural development in the normal and pathological neonatal rabbit brain. NIRS was used to follow changes in postnatal cerebral hemoglobin concentration and oxygenation. MRI was used to follow changes with age in surface-to-brain and cortical thickness, myelination progression, and brain water content as well as to stage the ischemic brain injury due to hypoxia ischemia.

2 Materials and Methods

2.1 NIRS System

NIRS measurements were performed with a frequency-domain tissue spectrometer³⁷ (Model No. 96208, ISS, Inc., Champaign, Illinois). This instrument uses two parallel photomultiplier tube detectors (PMTs) and 16 time-shared laser diodes (eight emitting at 690 nm and eight emitting at 830 nm). The frequency of intensity modulation is 110 MHz, and heterodyne detection was performed with a cross-correlation frequency of 5 kHz. Laser diodes and PMTs are coupled to fiber optics. The optical fibers are arranged in two identical flexible plastic probes. Each probe consists of one fiber bundle (made of five 400- μ m multimode glass fibers) con-

nected to a PMT detector and four fiber bundles (each made of two 400- μ m multimode glass fiber) connected to eight lasers. The tips of the illuminating and collecting fiber bundles in each probe are arranged along a line, with the source fibers at distances of 0.5, 0.8, 1.1, and 1.5 cm from the collecting bundle. The lasers are multiplexed at a rate of 100 Hz, so that an entire cycle over the eight sources is completed in 80 ms. We used the frequency-domain multidistance method for the quantitative measurement of the absorption (μ_a) and reduced scattering (μ_s') coefficients of brain tissue.³⁸ From the absorption coefficient measured at two wavelengths, the absolute values of the oxy-hemoglobin concentration ([HbO₂]), deoxy-hemoglobin concentration ([HbR]), total hemoglobin concentration ([HbT]), and hemoglobin saturation ([StO₂]) were calculated. The numeric values found for HbO₂, HbR, HbT, and StO₂ using the NIRS method reflect blood found in the microvasculature, i.e., chiefly in the capillaries, with some contribution from the venules and arterioles.³⁹

2.2 MRI System

MRI was performed on a 4.7-T small-bore GE Omega scanner using two different gradient sets depending on the animal age [8 cm i.d., 80 G/cm for ages up to post natal day 21 (P21) and 22 cm i.d., 7 G/cm for age P46]. A transmit/receive surface rf coil was used to acquire MRI scans according to the protocols described in Sect. 3.2. Animals were anesthetized during scanning, and were positioned in a purpose-built plastic holder that supported the animal's body in a prone position. The head was held within a contoured thermoplastic head holder under the receiver coil. Temperature was maintained within the magnet using a circulating warm water pad, and rectal temperature, heart rate, and oxygen saturation SaO₂ (by pulse oximetry) were measured and recorded continuously throughout scanning.

3 Animals and Measurement Protocols

Four groups of animals were used in this study: (1) normal control animals whose brains were scanned using NIRS, (2) normal control animals whose brains were scanned using MRI, (3) hypoxia-ischemia (HI) and HI control animals (surgical ligation of one common carotid artery only) whose brains were scanned using both NIRS and MRI, and (4) normal control animals from which blood was drawn at different time points to measure the hemoglobin spectrum.

3.1 Normal Control Group, Group 1: NIRS Measurements

Optical measurements were performed on eight normal control rabbits, from the same litter, every 2 to 3 days from 3 days (P3, i.e., postnatal day 3) to 60 days (P60) of age. Before the optical measurements the animals were shaved and weighed. Data were acquired at two wavelengths and from four source-detector separation distances with two identical probes. Each probe was calibrated against a silicon phantom of known optical properties to calibrate the light emitted by the eight laser sources. The probe consisted of a small piece of rubber to which the fibers were permanently fixed with epoxy. To mark the probe's position for easy day-to-day repositioning, within the initial test area of the rabbit's head, during subsequent experiments a rectangular area of fur (of the

same dimension of the probe) was shaved at the start of the study and this area was shaved again before every subsequent measurement. The measurements were performed while the animals were awake and one experimenter held each rabbit to keep it still. A second experimenter placed the optical probe in contact with the rabbit's scalp. This experimenter made sure the probe was in good contact with the skin, holding it in position and applying slight pressure. The probe was randomly positioned to the left and right of the midline taking care to avoid the sagittal sinus. Data collection did not begin until the animal was relaxed and still. Data were acquired for 8 s, and then the probe was lifted and repositioned over the shaved area of the head. The procedure was repeated 10 times with each probe. The optical measurements lasted about 3 to 5 min for each animal. Immediately after the measurements, the animals were returned to their mother's care. Optical measurements of the brain were taken on these animals three times per week from *P3* to *P60* days (2 months). The rabbits' arterial oxygenation saturation and heart rate were measured using a commercial pulse oximeter fitted with a neonatal sensor.

3.2 Normal Control Group, Group 2: MRI Measurements

A second litter of animals ($n=3$) was used to measure normal brain development. MRI measurements of the brains were taken using the following imaging parameter, in all cases in the coronal plane: spin-echo, echo-planar imaging (EPI) diffusion-weighted images (images show areas of tissue undergoing membrane depolarization, i.e., acute cell swelling, see also next section) were acquired in six noncollinear directions (diffusion tensor, DTI): field of view (FOV), 30 mm; 1-mm slice thickness; 64×64 pixels; echo time (TE), 45 ms; repetition time (TR), 8 s; and b value = 1450 in six directions. The T_2 mapping using EPI was also performed, with the same parameters as previously but with TE varied from 21 to 101 ms. The T_2 -weighted spin-echo images were also acquired: TE, 70 ms; TR, 4 s; FOV, 30 mm; 256×128 pixels; and 1-mm slice, eight slices. These animals were measured at the following time points: *P9*, *P14*, *P21*, and *P31*.

3.3 Hypoxia Ischemia (HI) Group, Group 3

A third litter of six rabbits was used for the HI experiments as described by D'Arceuil et al.⁴⁰ and were studied using both NIRS and MRI. Briefly, on day 9, all animals were anesthetized with 3% Isoflurane, and the right common carotid artery (CCA) was surgically isolated and ligated with 4.0 silk suture. Right CCA ligation results in the right brain hemisphere being more susceptible to suffer ischemia when the animal is subjected to hypoxia. The brains of CCA ligation or HI control animals have been shown in previous MRI studies to be the same as normal control animals and were measured with NIRS to ensure that there were no measureable differences in cerebral oxygenation as a result of the surgical CCA ligation. On *P10*, four of these animals were then anesthetized and received baseline MRI scans, as already described. Following baseline MRI scans, the HI insult was staged by using diffusion MRI to determine the duration of hypoxia as follows: serial dynamic diffusion weighted EPI scanning (TR, 3.2 s; TE, 45 ms; and 4 b values 0, 1450, 0, and 1450 along the Z

axis) was started approximately 5 min before initiation of hypoxia and continued for up to 3 h. Image data were stored to disk and then reconstructed in near real time, and the diffusion-weighted images were viewed on an offline computer screen which was updated approximately every 30 s.

Hypoxia was induced by reducing the fraction of inspired oxygen (FiO_2) by nitrogen dilution (the breathing gas mixture was switched to 60% nitrogen and 40% air, i.e., 8.4% FiO_2) and the anesthesia level maintained at between 0.65 and 1.0%. Arterial oxygen saturation was monitored carefully using a pulse oximeter. The extent of cellular depolarization within the brain was determined using diffusion weighted magnetic resonance (DWI) imaging, which is acutely sensitive to cell swelling.^{41,42} Acute cell swelling results in areas of hyperintensity in the DWI images or hypointensity in the fitted apparent diffusion coefficient (ADC) maps.⁴³ Images were acquired before, during, and after the hypoxic interval. Hypoxia was continued until diffusion hyperintensity was observed. At this point, hypoxia was reversed and scanning continued until the diffusion changes resolved completely. In this way, we define the duration of hypoxia not as a fixed time period but rather as the time required to achieve critical energy failure in the cells (and subsequently widespread membrane depolarization leading to reduced ADC, and hyperintensity on diffusion-weighted images). After recovery, follow-up scans were acquired (as for the normal animals) at *P17*, *P31* and *P43*.

Optical measurements of the brain were also taken on these animals once a week from *P3* to *P76* days (2.5 months). To investigate any differences in brain development due to preferential right brain hemisphere insult, the optical probes were positioned within both the right and left cerebral hemispheres and the measurements already described (in the normal control group) were repeated and data from each hemisphere were stored separately.

3.4 Blood Measurements, Group 4

A group of six animals (five neonates plus one adult) was used to measure maturational changes in the hemoglobin spectrum. Blood was drawn from *P3* ($n=1$), *P3* ($n=2$), *P10* ($n=1$), *P17* ($n=1$), and an adult. Blood taken from the neonates was a terminal procedure performed under deep anesthesia. Whole blood was heparinized and diluted with normal saline 1:100. These blood samples were 100% oxygenated having been exposed to the oxygen in the air as well as in the water used for dilution. In one case (*P17*), we added yeast to the diluted blood, sealed the cuvette, and obtained a hemoglobin spectrum of the deoxygenated blood sample.⁴⁴⁻⁴⁶ The spectral measurements were made using a fiberoptic spectrometer (S2000, Ocean Optics, Inc.) with a 100- μm slit and 600 lines/mm grating coupled with a 400- μm optical fiber. The light source used was a tungsten halogen lamp (LS-1, Ocean Optics, Inc.), coupled with another 400- μm optical fiber to deliver light to the sample. Absorption spectra of the blood samples contained in a 1-cm plastic cuvette were measured in the 530- to 1100-nm spectral range with an optical resolution of 4 nm.

3.5 Data Analysis: NIRS

The amplitude (ac) and phase (ph) data from four source-detector distances (ranging from 0.5 to 1.5 cm) were analyzed

using the frequency-domain (FD) multidistance method³⁸ to calculate absorption and reduced scattering coefficients at two wavelengths (690 and 830 nm). Using literature values for hemoglobin extinction coefficients,⁴⁷ we calculated the absolute values of oxy-, deoxy-, and total hemoglobin concentration, as well as the hemoglobin saturation. We corrected for water absorption assuming a percentage of 75% of water in the tissue. The frequency-domain multidistance method is appropriate for detecting optical properties of the underlying tissue for superficial layer thicknesses of up to 4 mm (Ref. 48). We verified that this holds for the range of distances used in this study, by performing preliminary experiments in layered phantoms, with various optical properties, and various thicknesses of the superficial layer. It takes only 80 ms to obtain a saturation measurement with the FD system in the configuration used. Because we were interested in the baseline optical properties, however, we averaged 100 points (i.e., 8 s). This reduced not only the instrumental noise, but also the contributions from physiological noise (i.e., slow and fast hemoglobin fluctuations due to arterial pulsation and respiration). We paid particular attention to the reproducibility of the optical measurements in each animal. Of the 20 measurements of 100 points each collected in each animal with two probes during every measurement session, we discarded the measurements for which (1) we had motion artifacts due to sudden movements of the animal; (2) the slopes of amplitude [$\ln(r^2ac)$] and phase versus distance were not straight lines ($R^2 < 0.95$), caused by nonuniform optical coupling of the probe with the head of the animal; (3) the blood parameters calculated from a measurement differed more than one standard deviation from the average of all of the measurements, because of imprecise positioning of the probe on the head of the animal. The average of the blood parameters for each measurement session was obtained by averaging the results over each rabbit group.

3.6 Data Analysis: MRI

MRI data fitting and handling were done using custom image data processing and display software (MRVision, MRVision Co., Winchester, Massachusetts). The serial DWI data acquired during hypoxia were processed at each scan time point. A two-point fit was performed on the signal intensity decay curves of the baseline (i.e., zero diffusion weighted) images (M_0 , with $b=0$) and diffusion weighted images (M , with $b=1450 \text{ s/mm}^2$), where the b value is a measure of the amount of diffusion sensitization applied and is dependent on the gradient strength and timing parameters used.⁴⁹ Measurements of the distance in millimeters from scalp to brain, and cortical thickness were derived from the T_2 -weighted images in the rostral, middle, and caudal aspect of the head at P9, P17, P31, and P43.

The diffusion tensor data were processed to generate ADC trace maps and fractional anisotropy (FA) maps.⁵⁰

4 Results

The rabbit weights as a function of age are shown in Fig. 1 for the normal control group. On average, from 3 to 60 days of age, the rabbit weights increased from 0.1 to 1.7 kg. The weight increased linearly from day 3 to day 20, at a rate of 11 g/day ($R^2=0.98$). From day 21 to day 60, the growth rate

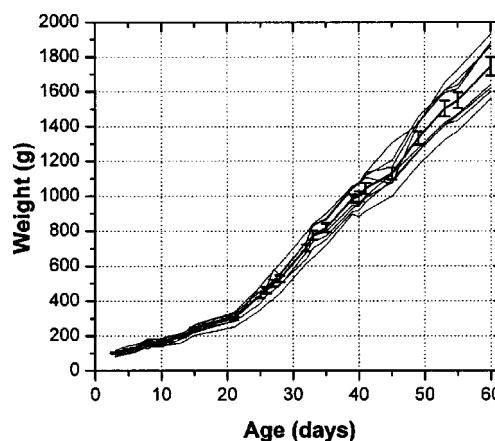


Fig. 1 Rabbit weights as a function of age (normal control group, $n=8$). The solid black curve represent the average weight $\pm 2SD$ (standard deviation), while the thin curves represent individual animals.

increased to 37 g/day ($R^2=1$). Arterial oxygenation ranged from 97 to 100%, and heart rate from 250 to 290 beats/minute.

4.1 NIRS Measurements

Reproducibility measurements on the phantom showed that by repositioning the probe randomly on the surface of the phantom, a maximum change of about 5% in the values of μ_a and μ_s' was seen. By repositioning the probe in the same location on the animals' heads there was, on average (across animals and days), an SD of 15% for μ_a and 10 to 20% for μ_s' ($\sim 20\%$) when the animals were very young (P3 to P30), $\sim 10\%$ when they were older (P30 to P60). This translates to a reproducibility of 15% for the measurement of StO_2 and HbT.

4.2 Normal Group: NIRS Data

For the normal group ($n=8$), the brain optical properties as a function of age are reported in Fig. 2. The absorption coefficient at 690 nm was significantly higher at 830 nm during the first month of life. This translates to a low tissue oxygenation during this period. The reduced coefficient was always higher at 690 than at 830 nm, as expected, and the changes in reduced scattering with age were not strongly correlated with the changes in absorption, except for the decrease at about P30.

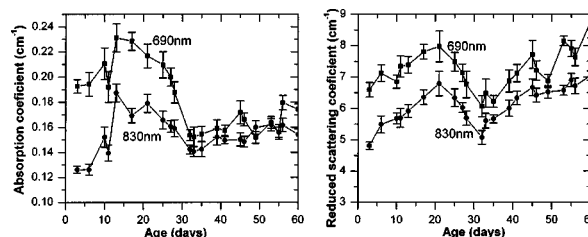


Fig. 2 Absorption (left) and reduced scattering (right) coefficients as a function of age (normal control group) measured with NIRS at two wavelengths (690 and 830 nm). The curves represent the average for eight animals and the error bars are the standard errors.

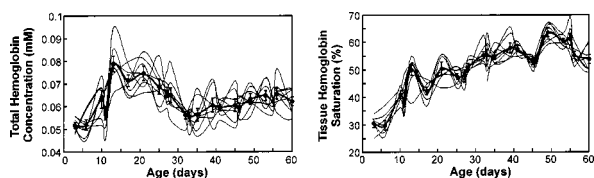


Fig. 3 Total hemoglobin concentration (left) and oxygenation (right) as a function of age (normal control group, $n=8$). The bold curves represent the average for all of the animals and the error bars are the standard errors. The thin curves represent the data for each individual rabbits.

Figure 3 shows hemoglobin concentration and oxygenation as a function of age for the control group. StO_2 increased significantly ($P<0.002$) in all animals (from about 30% at $P3$ to $P6$ to 53 to 63% at $P30$ to $P60$), while HbT also increased significantly ($P<0.003$) from day 3, peaked between $P13$ and $P21$ ($76 \mu\text{M}$, i.e., 0.076 mM) and showed a minimum at $P30$ to $P32$ ($65 \mu\text{M}$, i.e., 0.065 mM).

4.3 Normal Control Group: MRI Data

Figure 4 shows images from one slice in a representative normal control animal scanned at four time points from age $P0$ to $P31$. Figure 5 shows regions of interest (ROI) plots from this data in normal gray and white matter. Quantitative T_2 data were not acquired on day 0 in this animal (a T_2 -weighted EPI image is shown in the figure). Contrast in the diffusion anisotropy maps (FA) increased with age as the tissue became better myelinated, while ADC and T_2 contrast between GM and WM decreased (possibly due to the combined effects of white matter myelination and generally decreased tissue water content).

4.4 HI Group: NIRS Data

Measurements on the HI rabbits ($n=4$) and the HI controls ($n=2$) were performed less frequently than in the normal control group, but were continued up to $P76$. Figure 6 shows the results for HbT and StO_2 in the HI, HI control, and normal control groups. For figure clarity, the error bars (standard errors) for the HI controls are not shown. There were no apparent differences in total hemoglobin concentration and hemoglobin oxygenation between the normal, HI controls and HI groups from $P9$ to $P76$.

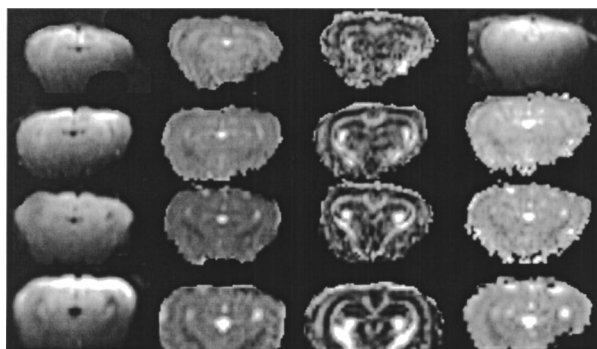


Fig. 4 Serial MRI data from one slice in a normal control rabbit brain. Images are (left to right) DWI, ADC, FA, and T_2 relaxation time maps. Time points are (top to bottom) $P9$, $P14$, $P21$, and $P31$.

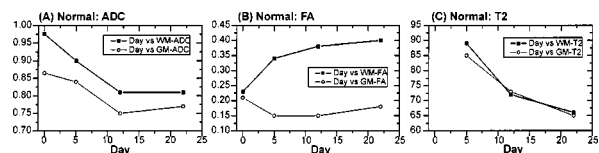


Fig. 5 ROI plots in normal cortical gray (GM) and white matter (WM) for apparent diffusion coefficient (a), fractional anisotropy (b), and T_2 (c) during development (ages $P9$ to $P31$) (T_2 values were not measured on day 0). The major changes are the increase in WM anisotropy (due to progressive myelination) and decrease in ADC and T_2 (due to decreased tissue water content).

4.5 HI Group: MRI Data

The ischemic tissue regions (regions of depolarization) appear as areas of hypointensity (black areas) in the ADC maps shown in Fig. 7, acquired at the peak of hypoxia. This animal showed bilateral ischemic changes throughout the cortex and some subcortical tissue bilaterally. These hypointense regions resolved back to baseline signal intensity during recovery (by approximately 30 min). All HI animals showed an area of depolarization covering essentially the entire cortex bilaterally ($19.47 \pm 6.14 \text{ mm}^2$). ADC decreased (on average to 50% of baseline) during HI and returned to baseline post HI. FA maps in this group showed that the animal brains were maturing as expected (i.e., same as in Fig. 5). Data for all animals were pooled and a paired, two-tailed, Student's t test was done to compare the FA values from the left and right cortex (GM). There was no significant difference between the pooled value in the left cortex compared with that of the right cortex; means \pm SD were 0.21 ± 0.04 and 0.22 ± 0.02 , respectively ($P=0.71$). An analysis of variance was performed on the data from the following timepoints to see whether the mean FA differed with age ($P0$, $P10$, $P17$, $P31$, and $P43$). There was no significant difference in FA with age ($P=0.71$).

The average distances from the scalp to the brain (in millimeters) in normal and HI groups were 1.16 ± 0.30 , 1.14 ± 0.38 , and 1.16 ± 0.38 in the rostral (front), middle, and caudal (back) aspects of the head from age $P10$ up to $P31$, and the average value did not differ among these three areas. The average distance from the scalp to the brain increased from age $P31$ to age $P43$ in the rostral, middle, and caudal aspects of the head, respectively; 2.17 ± 0.58 , 1.96 ± 0.41 , and 2.78 ± 1.23 . Cortical thickness (six rabbits from the HI experiment and two normals), measured from T_2 -weighted images, increased on average from 1.49 mm at $P10$ up to 2.36 mm at

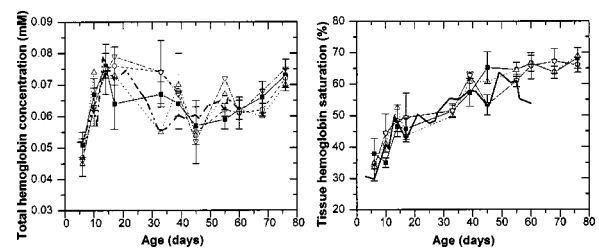


Fig. 6 Total hemoglobin concentration (left) and oxygenation (right) as a function of age for the three groups. CCA ligation was done on $P8$ and HI on $P9$.

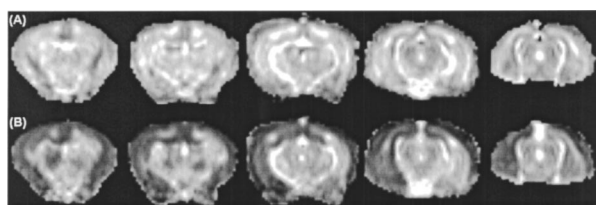


Fig. 7 (a) Baseline diffusion coefficient (ADC) images of the brain and (b) ADC images at the peak of hypoxia, taken from the serial diffusion data acquired during hypoxia. The cortex showed bilateral hypointensity in all aspects of the brain which completely reversed following the return to normoxia.

P43 (see Fig. 8). There were no differences between the average measurements in control and HI animals and data from both groups were pooled to generate Fig. 8.

4.6 Hemoglobin Spectra

Figure 9 shows the oxyhemoglobin spectra measured from blood samples taken from five neonatal rabbits and one adult in the 530 to 600-nm wavelength region. The characteristic HbO peaks for rabbits at different ages compared with that of humans⁵¹ are in agreement within experimental error (± 2 nm). Our data is also in agreement with that of Holter et al.⁵² who measured the hemoglobin spectra on neonatal (12 to 24 h old) and adult rabbits. Small differences between the spectra do not appear to be correlated to the animal age and could be due to different reduced properties of the samples. The deoxyhemoglobin spectra measured in the 17-day-old rabbit showed characteristic deoxyhemoglobin peaks at 555 and 758 nm, again within experimental error with respect to the human deoxygenated Hb spectrum (results not shown).

5 Discussion

We have demonstrated the potential of NIRS to be used in longitudinal studies to monitor brain hemoglobin oxygenation changes with brain maturation. Our results have shown reproducible measures of brain optical properties in 14 neonatal rabbits. Currently there are no methods that can be used to measure tissue optical properties *in vivo*, and there are no published NIRS data of brain optical properties in rabbits. Nevertheless, our measured optical properties are consistent with optical properties measured in piglet and in human brain.^{53–55}

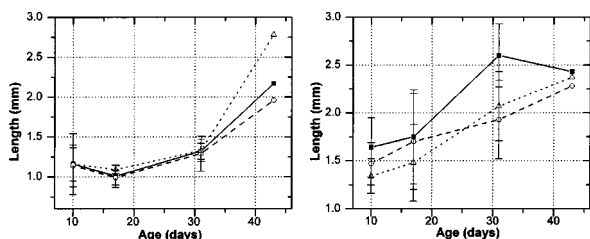


Fig. 8 Average changes in scalp-to-brain and cortical thickness ($n = 8$) measured in the MRI images at P10, P17, P31, and P43. Error bars represent the SD of the mean of six measures: two taken in the rostral, two in the middle, and two in the caudal aspects of the brain, respectively.

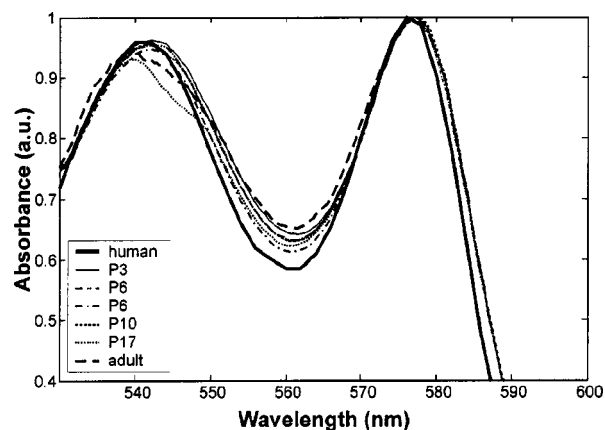


Fig. 9 Oxyhemoglobin spectra measured from blood samples taken from five neonatal rabbits (at ages 3, 6, 10, and 17 days, respectively) (thin curves) and one adult rabbit (thick dashed line) compared to a human oxyhemoglobin spectrum (thick solid line) in the 530 to 600-nm spectral region. The spectra are normalized to maximum and minimum values for easier comparison.

In this study, we used the diffusion equation applied to the model of a semi-infinite homogeneous medium to calculate the optical properties of brain tissue. The head of the rabbit is small, curved, and layered and is not a semi-infinite homogeneous medium, for which this model is valid, and as such there are errors that are inherent in our approximation, e.g., we expect that the surface layers of the head (skin, bone) could introduce some error in the measured optical properties of the brain. However, phantom studies reported in the literature⁴⁸ have shown that when the FD multidistance method is used, superficial layers of thickness, 4 mm and smaller, do not affect the measurements of the deeper layers. In addition, we performed additional experiments using layered phantoms, with similar optical properties to brain tissue (data not shown), with the range of distances used in our experiment, to further verify that our optical signals were being measured from brain tissue.

From the anatomical MRI measurements we verified that the overall thickness of the superficial layers of skin, scalp, and skull (on the rabbits' heads) was never larger than 3 mm, and therefore sufficiently small to be neglected. Moreover, by using only two source-detector distances of the four available to calculate the optical properties in the brain, we obtained the same results. Specifically, using any of the following three source-detector distance combinations 0.5 to 0.8, 0.8 to 1.1, and 1.1 to 1.5 cm, we obtained optical measurements that were within experimental error. The 0.8- to 1.1-cm set yielded results closest to those obtained by using the combination of all the four distances. The results reported in this paper are those obtained using all source detector distances.

Loss of light laterally, due to the small size of the head of the animal, can effectively result in increased measured absorption coefficients. This problem was minimized by using a small range of source-detector distances (0.5 to 1.5 cm) and our data do not seem to have been affected by this problem. In fact, the increasing absorption coefficients in the first few days of life, when the head size also increases, is opposite to what we would expect. The combined contribution of lateral loss of light and increased measured μ_a should be maxi-

imum when the head is smaller, i.e., at *P3* and *P6*, not at *P13*, where the absorption peaks (see Fig. 3).

The inhomogeneity of the rabbit's head and the use of small source-detector distances can cause crosstalk between the absorption and reduced scattering coefficients. In our measurements, the crosstalk between μ_a and μ_s' does not seem to be significant. In fact, μ_a and μ_s' at 690 nm are not correlated ($r=0.28$) and μ_a and μ_s' at 830 nm are weakly correlated ($r=0.57$), while, as expected, μ_s' at the two different wavelengths are correlated ($r=0.82$). In contrast, during brain development, absorption at different wavelengths is not necessarily correlated and we found μ_a at 690 nm and μ_a at 830 nm to be weakly correlated ($r=0.47$). This results because the independent changes in blood volume and oxygenation influence the absorption at these two wavelengths.

The value of cerebral hemoglobin oxygenation during the first 15 days of life is lower than what is usually measured in piglets⁵⁶ or term human neonates.⁵⁷ At birth, the rabbit brain is immature and is comparable to the brain of a premature human infant (24 to 32 weeks gestation). In fact, the piglet brain at birth is more mature than that of a term human neonate. As such, the data measured in the term human and the piglet brains are not directly comparable to that measured in the neonatal rabbit brain. In the following paragraphs, we outline some reasons for the low optically measured StO_2 within the first 30 postnatal days (Fig. 4) in neonatal rabbit brain.

One possible explanation for this low StO_2 value could have been the use of the extinction coefficients of hemoglobin derived from human studies, which were used to compute the hemoglobin concentrations in rabbit brain. However, this is unlikely because our measurements of blood samples taken at various ages from *P3* to adult showed no differences between the hemoglobin absorption spectra of neonatal rabbits, adult rabbits, and humans. Moreover, the values of the peripheral arterial oxygenation measured with the pulse oximeter on the neonatal rabbits were, as expected, 97 to 100%. If the neonatal hemoglobin spectra differed substantially from that of human hemoglobin, the SaO_2 measured by the pulse oximeter would also be affected, possibly resulting in lower than normal readings. Another possible reason is the presence of an additional, unknown absorber in the neonatal brain that affects the quantification of the hemoglobin concentration resulting in low StO_2 . This issue cannot be addressed in this study and may be addressed in future in another NIRS study that uses more than two wavelengths of light.

It is also possible that at this particular stage of the brain's development a low StO_2 is perfectly normal given the immature state of the brain and the rigors of the birthing process. During the birthing process the fetus experiences "normal birth asphyxia" due to the repeated reduction in uterine blood flow as a result of uterine contractions. Hence, the fetus is born in a state of "physiological asphyxia," which is normally relieved after the newborn takes the first few breaths. Newborn rabbits, like other newborn animals and humans, must undergo certain essential adjustments directly after birth. The transition to extrauterine life involves the following two major events: (1) establishment of the neonatal circulation and (2) establishment of the pulmonary circulation. It has been reported in the literature that at birth there is globally decreased cerebral blood flow (CBF) and in newborn lambs, humans,

and rabbits the cortex is preferentially supplied with blood. CBF is tailored to meet the energy and oxygen demands of the brain tissue.⁵⁸

There is very little myelination in the neonatal rabbit's brain and the cortical vasculature is immature. CBF and glucose utilization (i.e., oxidative capacity) are low. Tuor³¹ and Tuor et al.³⁵ using autoradiographic methods, showed that capillary density, oxidative metabolism, and local CBF change with development in the neonatal rabbit brain. Directly after birth (days 1 and 2), CBF is low and varies regionally. By day 17, there was markedly increased CBF (200 to 350%) compared to days 1 and 2, and CBF continued to increase in most brain regions up to 40 days postnatally. In these animals, capillary density increased from birth and matured to couple with cerebral metabolism at about postnatal day 17 then showed no significant change thereafter.

StO_2 measured optically reflects the balance between oxygen delivery and consumption in the tissue microvasculature, i.e., chiefly in the capillaries. In neonatal rabbits, the immaturity of the brain at birth, the low cerebral blood flow and glucose utilization coupled with the adjustment to extrauterine life and the immaturity of the brain is the likely explanation for the low measured StO_2 (on average 30% at *P3*). Thereafter, StO_2 increased with postnatal age (up to *P76*) as the brain matures structurally and functionally and the animals become adjusted to postnatal life. This result is in keeping with data published on premature human neonates which reported low StO_2 values at birth⁵⁹ (StO_2 values within the first 1 to 3 days of life were 50, 66, and 76% respectively).

HbT measured optically reflects blood volume in the illuminated tissue and is indirectly correlated to capillary density. In our measurements, HbT peaked at *P17*, consistent with an initial capillary density increase in the first 20 postnatal days reported by Tuor et al.³⁵ After this period when the microvasculature matures, tissue volume and vasculature both increase, resulting in constant HbT. However, local cerebral blood flow autoregulation depends on the maturity of the tissue and is not optimum below *P17*. These maturational changes support our optical data which showed a peak HbT between 15 and 17 days with no significant change thereafter, supporting a model of evolving, i.e., increasing, resting blood flow.

From our optical measurements, there were no differences, compared to normal controls, in tissue hemoglobin oxygenation or total hemoglobin concentration in brain tissue that suffered transient HI. Similarly, the longitudinal MRI data did not show appreciable differences in these two groups. However, the serial T_2 and diffusion MRI data clearly demonstrated the major structural changes going on in the maturing tissue. The deep WM structures, subcortical WM, corpus callosum, and internal capsule, showed increased FA up to *P31*, indicative of continuing myelination (Fig. 6). This same process is also likely the cause of a sustained reduction in free water content in both gray and white matter, resulting in the progressively decreased T_2 and ADC in these tissues.

Previous work in this HI model³³ showed that there are selective, bilateral ischemic changes in the CA1/CA2 and CA3 cortical brain regions and in the periventricular WM, which were significantly greater on the side of ligation. These changes were not associated with inflammatory necrotic but rather apoptotic changes. The area of tissue measured in the HI and in the normal control animals may be somewhat dif-

ferent due to some selective cell loss, i.e., we were measuring a population of cells with normal oxygenation. Our method may not be able to detect such small changes in the cerebral tissue oxygenation after HI. The fact that we measured these animals directly after (P10) then 1 week later may also mean that we may have missed the window where the apoptotic cells were cleared swiftly and surgically from the surrounding brain tissue. Also, it has to be considered that this may in fact suggest that a moderate (as shown from previous histological data³³) and transient ischemic insult such as this may not have resulted in permanent changes in tissue oxygenation and blood volume.

6 Conclusions

In human brain metabolism, myelination, vascularization, and neuronal and synaptic plasticity change rapidly in the first year of life. NIRS is an optimal technique to measure cerebral hemoglobin concentration and oxygenation in both animals and human neonates. Our longitudinal studies in neonatal rabbits demonstrated the feasibility of this method for safe, non-invasive measurement of cerebral oxygenation. Our results are in agreement with previous invasive studies. StO₂ measured optically, which reflects the balance between oxygen delivery and consumption in the tissue microvasculature, increased steadily up to P76. O₂ consumption in the maturing tissues increases in tandem with increased capillary density and blood flow. HbT reflects increasing blood volume which peaked at P17 as expected since the capillary density increases mostly during this period when the microvasculature finally matures. Thereafter, the increase in the cerebral vasculature is matched by increased cerebral tissue volume, resulting in constant blood volume. Serial MRI measurements provide complementary microstructural information to the cerebral oxygenation data acquired by NIRS. Indeed, incorporating the MRI structural data into a more complex model of light scattering may improve the analysis of the NIRS data in future. A more severe HI insult that results in secondary energy failure 24 to 72 h after recovery may lend some new insights into the dynamics of pathological cerebral hemodynamics during brain maturation in this model. Future work will concentrate on more severe insults with more frequent NIRS and MRI measurements.

Acknowledgments

We would like to thank René Michels and Felipe Jain for technical assistance during the measurements and David Boas and Enrico Gratton for helpful discussions. This research was supported by the U.S. National Institutes of Health (NIH) Grant No. RO1-HD42908. This work was also made possible through the inspiration and generous support of George Cowan.

References

1. A. G. Osborn, "Normal brain development and general classification of congenital malformations," in *Diagnostic Neuroradiology*, A. S. Patterson, Ed., pp. 3–14, Mosby, St. Louis, MO (1994).
2. A. Kinnala, H. Suhonen-Polvi, T. Aarimaa, P. Kero, H. Korvenranta, U. Ruotsalainen, J. Bergman, M. Haaparanta, O. Solin, P. Nuutila, and U. Wegelius, "Cerebral metabolic rate for glucose during the first six months of life: an FDG positron emission tomography study," *Arch. Dis. Child Fetal Neonatal Ed.* **74**, F153–157 (1996).
3. H. T. Chugani, "A critical period of brain development: studies of cerebral glucose utilization with PET," *Prev. Med.* **27**, 184–188 (1998).
4. A. M. Tokumaru, A. J. Barkovich, T. O'Uchi, T. Matsuo, and S. Kusano, "The evolution of cerebral blood flow in the developing brain: evaluation with iodine-123 iodoamphetamine SPECT and correlation with MR imaging," *AJNR Am. J. Neuroradiol.* **20**, 845–852 (1999).
5. T. Takahashi, R. Shirane, S. Sato, and T. Yoshimoto, "Developmental changes of cerebral blood flow and oxygen metabolism in children," *AJNR Am. J. Neuroradiol.* **20**, 917–922 (1999).
6. H. T. Chugani and M. E. Phelps, "Maturational changes in cerebral function in infants determined by 18FDG positron emission tomography," *Science* **231**, 840–843 (1986).
7. H. T. Chugani and M. E. Phelps, "Imaging human brain development with positron emission tomography," *J. Nucl. Med.* **32**, 23–26 (1991).
8. J. S. Wyatt, M. Cope, D. T. Delpy, S. Wray, and E. O. R. Reynolds, "Quantification of cerebral oxygenation and haemodynamics in sick newborn infants by near infrared spectrophotometry," *Lancet* **ii**, 1063–1066 (1986).
9. D. A. Benaron, W. E. Benitz, R. A. Ariagno, and D. K. Stevenson, "Noninvasive methods for estimating in vivo oxygenation," *Clin. Pediatr. (Phila)* **31**, 258–273 (1992).
10. L. Skov, O. Pryds, G. Greisen, and H. Lou, "Estimation of cerebral venous saturation in newborn infants by near infrared spectroscopy," *Pediatr. Res.* **33**, 52–55 (1993).
11. C. W. Yoxall, A. M. Weindling, N. H. Dawani, and I. Peart, "Measurement of cerebral venous oxyhemoglobin saturation in children by near-infrared spectroscopy and partial jugular venous occlusion," *Pediatr. Res.* **38**, 319–323 (1995).
12. K. Isobe, T. Kusaka, K. Nagano, K. Okubo, S. Yasuda, M. Kondo, S. Itoh, and S. Onishi, "Functional imaging of the brain in sedated newborn infants using near infrared topography during passive knee movement," *Neurosci. Lett.* **299**, 221–224 (2001).
13. J. H. Meek, M. Firbank, C. E. Elwell, J. Atkinson, O. Braddick, and J. S. Wyatt, "Regional hemodynamic responses to visual stimulation in awake infants," *Pediatr. Res.* **43**, 840–843 (1998).
14. K. Sakatani, S. Chen, W. Lichty, H. Zuo, and Y. P. Wang, "Cerebral blood oxygenation changes induced by auditory stimulation in newborn infants measured by near infrared spectroscopy," *Early Hum. Dev.* **55**, 229–236 (1999).
15. M. Bartocci, J. Winberg, G. Papendieck, T. Mustica, G. Serra, and H. Lagercrantz, "Cerebral hemodynamic response to unpleasant odors in the preterm newborn measured by near-infrared spectroscopy," *Pediatr. Res.* **50**, 324–330 (2001).
16. M. C. Ballesteros, P. E. Hansen, and K. Soila, "MR imaging of the developing human brain. Part 2. Postnatal development," *Radiographics* **13**, 611–622 (1993).
17. Y. Konishi, K. Hayakawa, M. Kuriyama, Y. Fujii, M. Sudo, K. Konishi, and Y. Ishii, "Developmental features of the brain in preterm and fullterm infants on MR imaging," *Early Hum. Dev.* **34**, 155–162 (1993).
18. Y. Fujii, Y. Konishi, M. Kuriyama, M. Maeda, M. Saito, Y. Ishii, and M. Sudo, "MRI assessment of myelination patterns in high-risk infants," *Pediatr. Neurol.* **9**, 194–197 (1993).
19. Y. Konishi, M. Kuriyama, K. Hayakawa, K. Konishi, M. Yasujima, Y. Fujii, M. Sudo, and Y. Ishii, "Magnetic resonance imaging in preterm infants," *Pediatr. Neurol.* **7**, 191–195 (1991).
20. K. Hayakawa, Y. Konishi, M. Kuriyama, K. Konishi, and T. Matsuda, "Normal brain maturation in MRI," *Eur. J. Radiol.* **12**, 208–215 (1991).
21. M. Battin, E. F. Maalouf, S. Counsell, A. H. Herilhy, and A. D. Edwards, "Magnetic resonance imaging of the brain of premature infants," *Lancet* **349**, 1741 (1997).
22. E. F. Maalouf, S. Counsell, M. Battin, and F. M. Cowan, "Magnetic resonance imaging of the neonatal brain," *Hosp. Med.* **59**, 41–45 (1998).
23. P. E. Hansen, M. C. Ballesteros, K. Soila, L. Garcia, and J. M. Howard, "MR imaging of the developing human brain. Part 1. Prenatal development," *Radiographics* **13**, 21–36 (1993).
24. H. Yamada, N. Sadato, Y. Konishi, K. Kimura, M. Tanaka, Y. Yonekura, and Y. Ishii, "A rapid brain metabolic change in infants detected by fMRI," *NeuroReport* **8**, 3775–3778 (1997).
25. T. Morita, T. Kochiyama, H. Yamada, Y. Konishi, Y. Yonekura, M. Matsumura, and N. Sadato, "Difference in the metabolic response to

- photic stimulation of the lateral geniculate nucleus and the primary visual cortex of infants: a fMRI study," *J. Neurosci. Res.* **38**, 63–70 (2000).
26. A. P. Born, M. J. Miranda, E. Rostrup, P. B. Toft, B. Peitersen, H. B. Larsson, and H. C. Lou, "Functional magnetic resonance imaging of the normal and abnormal visual system in early life," *Neuropediatrics* **31**, 24–32 (2000).
 27. A. P. Born, E. Rostrup, M. J. Miranda, H. B. Larsson, and H. C. Lou, "Visual cortex reactivity in sedated children examined with perfusion MRI (FAIR)," *Magn. Reson. Imaging* **20**, 199–205 (2002).
 28. P. Born, H. Leth, M. J. Miranda, E. Rostrup, A. Stensgaard, B. Peitersen, H. B. Larsson, and H. C. Lou, "Visual activation in infants and young children studied by functional magnetic resonance imaging," *Pediatr. Res.* **44**, 578–583 (1998).
 29. P. Born, E. Rostrup, H. Leth, B. Peitersen, and H. C. Lou, "Change of visually induced cortical activation patterns during development," *Lancet* **347**, 543 (1996).
 30. T. E. Inder, S. J. Wells, N. B. Mogridge, C. Spencer, and J. J. Volpe, "Defining the nature of the cerebral abnormalities in the premature infant: a qualitative magnetic resonance imaging study," *J. Pediatr. (St. Louis)* **143**, 171–179 (2003).
 31. U. I. Tuor, "Local cerebral blood flow in the newborn rabbit: an autoradiographic study of changes during development," *Pediatr. Res.* **29**, 517–523 (1991).
 32. U. I. Tuor, M. R. Del Bigio, and P. D. Chumas, "Brain damage due to cerebral hypoxia/ischemia in the neonate: pathology and pharmacological modification," *Cerebrovasc Brain Metab. Rev.* **8**, 159–193 (1996).
 33. H. D'Arceuil, W. Rhine, A. de Crespigny, M. Yenari, J. F. Tait, W. H. Strauss, T. Engelhorn, A. Kastrup, M. Moseley, and F. G. Blankenberg, "99mTc annexin V imaging of neonatal hypoxic brain injury," *Stroke* **31**, 2692–2700 (2000).
 34. R. F. Keep and H. C. Jones, "Cortical microvessels during brain development: a morphometric study in the rat," *Microvasc. Res.* **40**, 412–426 (1990).
 35. U. I. Tuor, G. Kurpita, and C. Simone, "Correlation of local changes in cerebral blood flow, capillary density, and cytochrome oxidase during development," *J. Comp. Neurol.* **342**, 439–448 (1994).
 36. H. T. Chugani, D. A. Hovda, J. R. Villablanca, M. E. Phelps, and W. F. Xu, "Metabolic maturation of the brain: a study of local cerebral glucose utilization in the developing cat," *J. Cereb. Blood Flow Metab.* **11**, 35–47 (1991).
 37. S. Fantini, M. A. Franceschini, J. S. Maier, S. A. Walker, B. Barbieri, and E. Gratton, "Frequency-domain multichannel optical detector for non-invasive tissue spectroscopy and oximetry," *Opt. Eng.* **34**, 32–42 (1995).
 38. S. Fantini, M. A. Franceschini, J. B. Fishkin, B. Barbieri, and E. Gratton, "Quantitative determination of the absorption spectra of chromophores in strongly scattering media: a light-emitting-diode based technique," *Appl. Opt.* **33**, 5204–5213 (1994).
 39. H. Liu, B. Chance, A. H. Hielscher, S. L. Jacques, and F. K. Tittel, "Influence of blood vessels on the measurement of hemoglobin oxygenation as determined by time-resolved reflectance spectroscopy," *Med. Phys.* **22**, 1209–1217 (1995).
 40. H. E. D'Arceuil, A. J. Crespigny, J. Rother, M. Moseley, and W. Rhine, "Serial magnetic resonance diffusion and hemodynamic imaging in a neonatal rabbit model of hypoxic-ischemic encephalopathy," *NMR Biomed.* **12**, 505–514 (1999).
 41. M. E. Moseley, Y. Cohen, J. Mintorovitch, L. Chileuit, H. Shimizu, J. Kucharczyk, M. F. Wendland, and P. R. Weinstein, "Early detection of regional cerebral ischemia in cats: comparison of diffusion- and T2-weighted MRI and spectroscopy," *Magn. Reson. Med.* **14**, 330–346 (1990).
 42. A. J. de Crespigny, J. Rother, C. Beaulieu, M. E. Moseley, and M. Hoehn, "Rapid monitoring of diffusion, DC potential, and blood oxygenation changes during global ischemia. Effects of hypoglycemia, hyperglycemia, and TTX," *Stroke* **30**, 2212–2222 (1999).
 43. H. E. D'Arceuil, A. J. de Crespigny, J. Rother, S. Seri, M. E. Moseley, D. K. Stevenson, and W. Rhine, "Diffusion and perfusion magnetic resonance imaging of the evolution of hypoxic ischemic encephalopathy in the neonatal rabbit," *J. Magn. Reson. Imaging* **8**, 820–828 (1998).
 44. B. Chance, S. Leigh, H. Miyake, D. S. Smith, S. Nioka, R. Greenfield, M. Finander, K. M. Kaufmann, W. Levy, M. Young, P. Cohen, H. Yoshioka, and R. Boretsky, "Comparison of time-resolved and unresolved measurements of deoxyhemoglobin in brain," *Proc. Natl. Acad. Sci. U.S.A.* **85**, 4971–4975 (1998).
 45. H. Y. Ma, C. W. Du, and B. Chance, "A homodyne frequency-domain instrument phase detection system—I&Q phase detection system," *Proc. SPIE* **2979**, 826–837 (1997).
 46. S. Srinivasan, W. Pogue, S. Jiang, H. Dehghani, C. Kogel, S. Soho, J. J. Gibson, D. Tosteson, S. P. Poplack, and K. D. Paulsen, "Interpreting hemoglobin and water concentration, oxygen saturation, and scattering measured in vivo by near-infrared breast tomography," *Proc. Natl. Acad. Sci. U.S.A.* **100**, 12349–12354 (2003).
 47. S. Wray, M. Cope, and D. T. Delpy, "Characteristics of the near infrared absorption spectra of cytochrome aa3 and hemoglobin for the noninvasive monitoring of cerebral oxygenation," *Biochim. Biophys. Acta* **933**, 184–192 (1988).
 48. M. A. Franceschini, S. Fantini, L. A. Paunescu, J. S. Maier, and E. Gratton, "Influence of a superficial layer in the quantitative spectroscopic study of strongly scattering media," *Appl. Opt.* **37**, 7447–7458 (1998).
 49. D. Le Bihan, E. Breton, D. Lallemand, P. Grenier, E. Cabanis, and M. Laval-Jeantet, "MR imaging of intravoxel incoherent motions: application to diffusion and perfusion in neurologic disorders," *Radiology* **161**, 401–407 (1986).
 50. C. Pierpaoli and P. J. Basser, "Toward a quantitative assessment of diffusion anisotropy," *Magn. Reson. Med.* **36**, 893–906 (1996).
 51. S. Prah <http://omlc.ogi.edu/spectra/hemoglobin/summary.html>.
 52. P. H. Holter, P. Kierulf, and H. E. Refsum, "Haemoglobin O₂ binding in newborn and adult rabbits," *Acta Physiol. Scand.* **130**, 349–356 (1987).
 53. S. Fantini, D. Hueber, M. A. Franceschini, E. Gratton, W. Rosenfeld, P. G. Stubblefield, D. Maulik, and M. R. Stankovic, "Non-invasive optical monitoring of the newborn piglet brain using continuous-wave and frequency-domain methods," *Phys. Med. Biol.* **44**, 1543–1563 (1999).
 54. A. Sassaroli, F. Martelli, Y. Tanikawa, K. Araki, Y. Onodera, and Y. Yukio, "Time-resolved measurements of in vivo optical properties of piglet brain," *Opt. Rev.* **7**, 420–425 (2000).
 55. J. Choi, M. Wolf, V. Toronov, U. Wolf, C. Polzonetti, D. Hueber, L. P. Safonova, R. Gupta, A. Michalos, W. Mantulin, and E. Gratton, "Noninvasive determination of the optical properties of adult brain: near-infrared spectroscopy approach," *J. Biomed. Opt.* **9**, 221–229 (2004).
 56. D. M. Hueber, M. A. Franceschini, H. Y. Ma, Q. Zhang, J. R. Ball-esteros, S. Fantini, D. Wallace, V. Ntziachristos, and B. Chance, "Non-invasive and quantitative near-infrared haemoglobin spectrometry in the piglet brain during hypoxic stress, using a frequency-domain multidistance instrument," *Phys. Med. Biol.* **46**, 41–62 (2001).
 57. N. Nagdyman, T. Fleck, S. Barth, H. Abdul-Khaliq, B. Stiller, P. Ewert, M. Huebler, H. Kuppe, and P. E. Lange, "Relation of cerebral tissue oxygenation index to central venous oxygen saturation in children," *Intensive Care Med.* **30**, 468–471 (2004).
 58. A. S. King, "Fetal and neonatal circulation and respiration," in *Foundations of Veterinary Studies: The Cardiorespiratory System Integration of Normal and Pathological Structure and Function*, pp. 391–413, Blackwell Science Ltd. (1999).
 59. G. Naulaers, G. Morren, S. Van Huffel, P. Casaer, and H. Devlieger, "Cerebral tissue oxygenation index in very premature infants," *Arch. Dis. Child Fetal Neonatal Ed.* **87**, F189–192 (2002).